



PERGAMON

International Journal of Solids and Structures 40 (2003) 5865–5886

INTERNATIONAL JOURNAL OF  
**SOLIDS and  
STRUCTURES**

www.elsevier.com/locate/ijsostr

# In-plane free vibration and stability of loaded and shear-deformable circular arches

C.S. Huang <sup>a,\*</sup>, K.Y. Nieh <sup>b</sup>, M.C. Yang <sup>c</sup>

<sup>a</sup> Department of Civil Engineering, National Chiao Tung University, 1001 Ta-Hsueh Road, Hsinchu 30050, Taiwan

<sup>b</sup> Department of Civil Engineering, Tamkang University, Tamsui 25137, Taiwan

<sup>c</sup> Department of Civil Engineering, National Chiao Tung University, Hsinchu 30050, Taiwan

Received 25 June 2003; received in revised form 25 June 2003

---

## Abstract

The first known equations governing vibrations of preloaded, shear-deformable circular arches are derived according to a variational principle for dynamic problems concerning an elastic body under equilibrium initial stresses. The equations are three partial differential equations with variable coefficients. The governing equations are solved for arches statically preloaded with a uniformly distributed vertical loading, by obtaining a static, closed-form solution and an analytical dynamic solution from series solutions and dynamic stiffness matrices. Convergence to accurate results is obtained by increasing the number of elements or by increasing both the number of terms in the series solution and the number of terms in the Taylor expansion of the variable coefficients. Graphs of non-dimensional frequencies and buckling loads are presented for preloaded clamped arches. They clarify the effects of opening angle and thickness-to-radius ratio on vibration frequencies and buckling loads. The effects of static deformations on vibration frequencies are also investigated. This work also compares the results obtained from the proposed governing equations with those obtained from the classical theory neglecting shear deformation.

© 2003 Elsevier Ltd. All rights reserved.

---

## 1. Introduction

Curved beam structures have been extensively used in civil, mechanical, and aerospace engineering applications, including for example, arch bridges, springs, and stiffeners in aircraft structures. Research into the vibrations of curved beams began in the 19th century (Love, 1944), and over 500 references can be found in review articles (Markus and Nanasi, 1981; Laura and Maurizi, 1987; Chidamparam and Leissa, 1993), which reveal that most of the research addresses the vibrations in unloaded arches and rings. Even in the past decade, studies of arch vibrations focused on unloaded cases but with complicating effects. For example, Kawakami et al. (1995), Huang et al. (1998) and Oh et al. (1999) considered arches with variable curvature or cross-sections; Qatu (1993a,b) and Tseng et al. (2000) studied composite arches. Rather few

---

\* Corresponding author. Tel.: +886-3-5712121x54962; fax: 886-3-5716257.

E-mail address: cshuang@cc.nctu.edu.tw (C.S. Huang).

publications address the vibrations of loaded arches and rings, even though dynamic analyses of loaded arches are frequently required for a wide range of engineering applications.

For simplicity, most studies on the vibrations and stability of loaded circular arches consider cases with an inextensible centerline and no shear deformation. For example, Timoshenko and Gere (1961) obtained closed-form solutions for the buckling loads of pin-ended and fixed circular arches with uniformly distributed radial loading. Wempner and Kesti (1962) provided an analytical solution for the buckling load of a clamped circular arch under a uniform hydrostatic pressure, constant directional pressure or a centrally directed pressure. Gjelsvik and Bodner (1962) applied an energy-based method to evaluate the stability of a clamped arch under center point loading, while Schreyer and Masur (1966) exactly solved the non-linear equilibrium equations for an arch under a uniform load. Wasserman (1977) developed exact and approximate formulas for determining the lowest natural frequencies and critical loads of arches with flexibly supported ends. Plaut and Johnson (1981) investigated the effects of an elastic foundation and a sinusoidally distributed load on the natural frequencies of simply supported shallow arches, while Perkins (1990) correlated experimental results with theoretical analysis considering vibrations of an elastica arch under a large axial load. Both works considered the vibration about the deformed equilibrium state caused by a static load. Kang et al. (1996) used the differential quadrature method to determine the critical loads of circular arches.

Centerline extensibility is known to affect substantially the vibrations of rotating thick rings (Lin and Soedel, 1988). Chidamparam and Leissa (1995) applied the Ritz method to elucidate how centerline extensibility influences the in-plane free vibrations of loaded circular arches. However, they assumed an inextensible centerline when determining the initial axial force distribution along a circular arch under a static, distributed vertical load. Matsunaga (1996) developed a one-dimensional higher-order theory for arches with constant initial axial forces and used Fourier series expansion to determine the critical loads of simply-supported circular arches subjected to constant axial forces. Nieh et al. (2003) analytically solved the vibration and stability of a loaded elliptical arch, using a series solution along with dynamic stiffness matrix method. These studies ignored not only shear deformation but also static deformation.

Shear deformation must be considered for thick beams. The aforementioned studies indicate a need to develop equations that govern the free vibrations of a loaded circular arch that is shear-deformable. This work develops the governing equations using the variational form introduced by Washizu (1982) for the dynamical problems concerning an elastic body under initial stresses. The developed governing equations include not only the effect of the initial axial force but also the effects of other initial stress resultants, such as shear force and moment due to initial loading. The study also elucidates the effects of static deformations.

These equations are employed primarily to investigate free vibration and buckling analyses of a circular arch under uniform vertical loading. Developing analytical solutions involves two main steps. First, the static solution for the circular arch under loading is obtained in closed form. The vibration frequencies and buckling loads are then determined using the dynamic stiffness matrix method. A dynamic stiffness matrix is established by a series solution of the governing equations. The proposed solution is applied to elucidate the effects of the opening angle and the thickness-to-radius ratio on the vibration frequencies and buckling loads of loaded circular arches. The extent to which the magnitude of a uniformly distributed static load affects vibration frequencies is also considered. The effects of shear deformation on vibration frequencies and buckling loads are demonstrated by comparing the present results with the published data obtained by ignoring shear deformation. The effects of the static deformations on the vibration frequencies are also clarified.

## 2. Equations governing loaded free vibrations

Consider a part of a circular arch, as depicted in Fig. 1, with a centroidal radius  $R$ , and a thickness  $h$ . Polar coordinates  $r$  and  $\theta$  specify a point on the arch. The arch is initially subjected to static loading  $\gamma(\theta)$ .

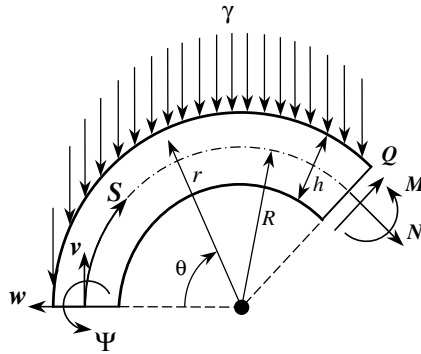


Fig. 1. A sketch of a loaded circular arch.

The cross-section of the arch is assumed to have at least one axis of symmetry so that in-plane motion is not coupled with out-of-plane motion. The ratio of  $h$  to  $R$  is assumed to be sufficiently small. A static load is assumed to induce initial stresses of  $\sigma_{ij}^{(0)}$  at equilibrium. The dynamic tangential and radial displacements of a point during the in-plane free vibration of a loaded arch are represented by  $\bar{v}$  and  $\bar{w}$ , respectively. Fig. 1 also presents the sign convention for positive dynamic displacement components, bending moment ( $M$ ), shear force ( $Q$ ), and axial force ( $N$ ).

This section presents three sets of governing equations for vibrations of loaded arches according to different assumptions. These equations can be classified by (1) the nature of the initial static equilibrium state, and (2) the influence of shear deformation. Three different theories for vibrations of a preloaded arch are presented below.

### 2.1. Shear deformable theory with initial shape (SDTIS)

In this theory, the arch under consideration is shear-deformable and deformations caused by static loading are assumed to be sufficiently small that their effect on the deformed curvature can be ignored. As in Timoshenko first-order beam theory, the in-plane displacement components of an arch can be assumed to be

$$\bar{v}(r, \theta, t) = v(\theta, t) - z\psi(\theta, t), \quad \bar{w}(r, \theta, t) = w(\theta, t), \tag{1}$$

where  $v$  and  $w$  represent the tangential and radial displacements of the centroidal axis, respectively, and  $\psi$  is the angle of rotation of the centroidal axis due to bending only. The coordinate  $z$  refers to the distance of a point from the centroidal axis, such that  $z = r - R$  and  $-h/2 \leq z \leq h/2$ . Under the displacement field described by Eq. (1), the non-zero dynamic strain components are  $\epsilon_{\theta\theta}$  and  $\epsilon_{r\theta}$ , which are related to the displacement components by the following equations.

$$\epsilon_{\theta\theta} = \epsilon_{\theta\theta}^{(L)} + \epsilon_{\theta\theta}^{(H)}, \tag{2a}$$

$$\epsilon_{r\theta} = \epsilon_{r\theta}^{(L)} + \epsilon_{r\theta}^{(H)}, \tag{2b}$$

$$\epsilon_{\theta\theta}^{(L)} = \frac{1}{r} \left( \frac{\partial v}{\partial \theta} - \frac{z \partial \psi}{\partial \theta} + w \right), \tag{2c}$$

$$\varepsilon_{\theta\theta}^{(H)} = \frac{1}{2r^2} \left[ \left( \frac{\partial v}{\partial \theta} - \frac{z \partial \psi}{\partial \theta} + w \right)^2 + \left( \frac{\partial w}{\partial \theta} - v + z \psi \right)^2 \right], \quad (2d)$$

$$\varepsilon_{r\theta}^{(L)} = \frac{1}{2} \left[ \frac{1}{r} \left( \frac{\partial w}{\partial \theta} - v + z \psi \right) - \psi \right], \quad (2e)$$

$$\varepsilon_{r\theta}^{(H)} = \frac{1}{2r} \left( \frac{\partial v}{\partial \theta} + w - \frac{z \partial \psi}{\partial \theta} \right) (-\psi), \quad (2f)$$

where the superscript “*L*” represents infinitesimal strain parts, while the superscript “*H*” denotes high-order terms.

In the following derivation, the dynamic deformation is assumed to be infinitesimal and the material is assumed to be elastic and isotropic. Hence, the dynamic stresses,  $\sigma_{ij}$ , are related to  $\varepsilon_{ij}^{(L)}$  by Hooke’s law for plane strain. The equations governing the free vibration of a loaded circular arch and the associated boundary conditions will be developed according to the following variational principle given by Washizu (1982) for solving the dynamic problem of an elastic body with equilibrium initial stresses.

$$\delta \int_{t_1}^{t_2} \left\{ T - U - \iiint_V \sigma_{ij}^{(0)} \varepsilon_{ij}^{(H)} dV \right\} dt = 0, \quad (3)$$

where  $T$  and  $U$  are the kinetic and strain energies, given by,

$$T = \iiint_V \frac{1}{2} \rho (\dot{v}^2 + \dot{w}^2) dV, \quad (4a)$$

$$U = \iiint_V \frac{1}{2} \sigma_{ij} \varepsilon_{ij}^{(L)} dV, \quad (4b)$$

$\rho$  is the material density, and the dots denote the derivative with respect to time. The term with  $\sigma_{ij}^{(0)}$  represents the additional strain energy contributed by the initial static stresses.

Introduce the following definition of stress resultants:

$$(N, M) = \int_A \sigma_{\theta\theta}(1, z) dA, \quad (5a)$$

$$Q = \int_A \sigma_{r\theta} dA, \quad (5b)$$

$$(N^{(0)}, M^{(0)}, P^{(0)}) = \int_A \sigma_{\theta\theta}^{(0)}(1, z, z^2) dA, \quad (5c)$$

$$(Q^{(0)}, T^{(0)}) = \int_A \sigma_{r\theta}^{(0)}(1, z) dA. \quad (5d)$$

The relationships between the stress resultants and the displacement components for an arch with  $h/R$  sufficiently less than unity are,

$$N = EA \left( \frac{\partial v}{\partial S} + \frac{w}{R} \right), \quad M = EI \frac{\partial \psi}{\partial S}, \quad Q = \kappa GA \left( \frac{\partial w}{\partial S} - \frac{v}{R} - \psi \right), \quad (6)$$

$$P = EI \left( \frac{\partial v}{\partial S} + \frac{w}{R} \right), \quad \text{and} \quad T = \kappa GI \frac{\psi}{R}$$

where  $S$  is the arc length coordinate (see Fig. 1);  $E$  and  $G$  are elastic and shear moduli, respectively;  $A$  and  $I$  are the area and moment of inertia of the cross-section, respectively, and  $\kappa$  is the correction factor for the shear force and equals 0.85 for a rectangular cross-section. Notably, in deriving the expression of  $P$  in terms of displacement components, it is assumed that the cross-section is symmetric about the line of  $z = 0$ .

By performing the variation as indicated in Eq. (3), the governing equations for the free vibrations of a statically loaded arch with the displacement field specified by Eq. (1) are obtained and expressed as

$$N' + \frac{Q}{R} + \left( N^{(0)}v' + M^{(0)}\psi' + \frac{N^{(0)}}{R}w - Q^{(0)}\psi \right)' + \frac{N^{(0)}}{R}w' - \frac{1}{R^2}(N^{(0)}v + M^{(0)}\psi) = \rho A \ddot{v}, \quad (7a)$$

$$Q' - \frac{N}{R} + \left( N^{(0)}w' - \frac{N^{(0)}}{R}v - \frac{M^{(0)}}{R}\psi \right)' - \frac{N^{(0)}}{R}v' - \frac{M^{(0)}}{R}\psi' + Q^{(0)}\frac{\psi}{R} - \frac{N^{(0)}}{R^2}w = \rho A \ddot{w}, \quad (7b)$$

$$M' + Q + \left( M^{(0)}v' + \frac{M^{(0)}}{R}w + P^{(0)}\psi' \right)' + \frac{M^{(0)}}{R}w' + Q^{(0)}\left(v' + \frac{w}{R}\right) - \frac{M^{(0)}}{R^2}v - \frac{P^{(0)}}{R^2}\psi + (T^{(0)})'\psi = \rho I \ddot{\psi}, \quad (7c)$$

and the associated boundary conditions are,

$$v = 0 \quad \text{or} \quad -N - N^{(0)}v' - M^{(0)}\psi' - \frac{N^{(0)}w}{R} + Q^{(0)}\psi = 0, \quad (8a)$$

$$w = 0 \quad \text{or} \quad -Q - N^{(0)}w' + \frac{N^{(0)}v}{R} + \frac{M^{(0)}\psi}{R} = 0, \quad (8b)$$

$$\psi = 0 \quad \text{or} \quad -M - M^{(0)}v' - \frac{M^{(0)}w}{R} - P^{(0)}\psi' - T^{(0)}\psi = 0, \quad (8c)$$

where the primes denote derivatives with respect to  $S$ .

## 2.2. Shear deformable theory with deformed state (SDTDS)

This theory considers a shear-deformable arch under a static loading, and vibrations of the arch about the statically deformed state. Restated, this theory additionally considers the effects of static deformations on the vibrations of the preloaded arch. The static deformations will cause changes in the initial circular shape of the arch, resulting in a change of the radius of the centroidal axis. Let  $R^*$  denote the radius of the statically deformed centroidal axis, and is no longer a constant but a function of  $S$ , determined from the static deformations by,

$$\frac{1}{R^*} = \frac{1}{R} - \left( (w^{(0)})' - \frac{v^{(0)}}{R} \right)', \quad (9)$$

where  $w^{(0)}$  and  $v^{(0)}$  are the static radial and tangential displacements, respectively.

Since Eqs. (6),(7a)–(7c), and (8a)–(8c) are expressed in terms of the independent variable  $S$ , these equations also apply in this theory, except that  $R$  in these equations is replaced by  $R^*$ .

### 2.3. Classical theory neglecting shear deformation (CTNSD)

This theory neglects shear deformation and rotary inertia and further considers a moderately small rotation in  $\varepsilon_{\theta\theta}^{(H)}$ , such that  $\varepsilon_{\theta\theta}^{(H)}$  in Eq. (2d) becomes

$$\varepsilon_{\theta\theta}^{(H)} = \frac{1}{2r^2} \left( \frac{\partial w}{\partial \theta} - v \right)^2. \quad (10)$$

Static deformations are also neglected. Hence, the corresponding governing equations can be derived following the procedure presented in Section 2.1:

$$-\frac{M'}{R} + N' + \frac{N^{(0)}}{R} \left( w' - \frac{v}{R} \right) = \rho A \ddot{v}, \quad (11a)$$

$$-M'' - \frac{N}{R} + \left[ N^{(0)} \left( w' - \frac{v}{R} \right) \right]' = \rho A \ddot{w}. \quad (11b)$$

Eqs. (11a) and (11b) are identical to those obtained by Chidamparam (1993), who used a perturbation technique. These two equations, unlike Eqs. (7a)–(7c), involve only the initial axial forces. Notably, Eqs. (11a) and (11b) cannot be directly deduced from Eqs. (7a)–(7c).

Two important differences exist between the shear deformable theory with initial shape (SDTIS) (Eqs. (7a)–(7c)) and this classical theory (Eqs. (11a) and (11b)). In computing static initial stress resultants, the former but not the latter considers shear deformation, so that  $N^{(0)}$  in Eqs. (7a)–(7c) may differ considerably from those in Eqs. (11a) and (11b) in some cases. In determining dynamic responses, the proposed theory addresses the effects of shear deformation, rotary inertia, and all initial stress resultants, while the classical theory considers only the effect of the initial axial force.

## 3. Solution

An analytical solution for the free vibration and stability of a circular arch with a rectangular cross-section, subjected to uniform vertical loading, is presented. This section will demonstrate the procedure of establishing the solution according to shear deformable theory with the deformed state, using Eqs. (7a)–(7c) but with  $R$  replaced by  $R^*$ . The solution is obtained in two main steps. The first is to determine the closed-form, static solution for the arch under uniformly distributed vertical loading (see Fig. 1). Then, the dynamic stiffness matrix approach, in conjunction with a series solution, is applied to determine the vibration frequencies of the arch.

### 3.1. Static solution

The equilibrium equations for a circular arch under uniform vertical loading, as depicted in Fig. 1, are

$$(N^{(0)})' + \frac{Q^{(0)}}{R} = \gamma \cos \theta, \quad (12a)$$

$$(Q^{(0)})' - \frac{N^{(0)}}{R} = \gamma \sin \theta, \quad (12b)$$

$$(M^{(0)})' + Q^{(0)} = 0. \quad (12c)$$

The general solutions for the stress resultants can be easily obtained by directly integrating the above equations with some mathematic manipulation (Yang, 2002):

$$Q^{(0)} = C_1 \cos \theta + C_2 \sin \theta + R\gamma\theta \sin \theta, \quad (13a)$$

$$N^{(0)} = -C_1 \sin \theta + C_2 \cos \theta + R\gamma\theta \cos \theta, \quad (13b)$$

$$M^{(0)} = -C_1 R \sin \theta + C_2 R \cos \theta - R^2 \gamma (\sin \theta - \theta \cos \theta) + C_3, \quad (13c)$$

where the coefficients  $C_1$ ,  $C_2$  and  $C_3$  are to be determined by the specified boundary conditions. The relationships between the stress resultants and the displacement components, following direct integration, yield

$$v^{(0)} = -C_3 \frac{R^2 \theta}{EI} + C_4 \cos \theta + C_5 \sin \theta - C_6 R + \delta_1 \theta \cos \theta + \delta_2 \theta \sin \theta + \delta_3 \theta^2 \cos \theta, \quad (14a)$$

$$w^{(0)} = \left( -C_1 \frac{R}{EA} + C_4 - \delta_2 \right) \sin \theta + \left( C_2 \frac{R}{EA} - C_5 - \delta_1 \right) \cos \theta + C_3 \frac{R^2}{EI} + \left( \frac{R^2 \gamma}{EA} - \delta_2 - 2\delta_3 \right) \theta \cos \theta + \delta_3 \theta^2 \sin \theta + \delta_1 \theta \sin \theta, \quad (14b)$$

$$\psi^{(0)} = \frac{R}{EI} \{ C_1 R \cos \theta + C_2 R \sin \theta + R^2 \gamma (2 \cos \theta + \theta \sin \theta) + C_3 \theta \} + C_6, \quad (14c)$$

where

$$\delta_1 = \frac{R}{2E} \left( \frac{1}{A} + \frac{E}{\kappa GA} + \frac{R^2}{I} \right) C_2, \quad (15a)$$

$$\delta_2 = \frac{1}{2} \left\{ -\frac{R}{E} \left( \frac{1}{A} + \frac{E}{\kappa GA} + \frac{R^2}{I} \right) C_1 + \frac{R^2 \gamma}{E} \left( \frac{1}{A} - \frac{2R^2}{I} \right) \right\} - \delta_3, \quad (15b)$$

$$\delta_3 = \frac{R^2 \gamma}{4E} \left( \frac{1}{A} + \frac{E}{\kappa GA} + \frac{R^2}{I} \right). \quad (15c)$$

Coefficients  $C_4$ ,  $C_5$  and  $C_6$  are also to be determined by the specified boundary conditions. The definitions of  $P^{(0)}$  and  $T^{(0)}$  and Eqs. (14a)–(14c) lead to

$$P^{(0)} = \frac{I}{A} (-C_1 \sin \theta + C_2 \cos \theta + R\gamma\theta \cos \theta), \quad (16a)$$

$$T^{(0)} = \frac{\kappa G}{E} \{ C_1 R \cos \theta + C_2 R \sin \theta + C_3 \theta + R^2 \gamma (2 \cos \theta + \theta \sin \theta) \} + C_6 \frac{\kappa G I}{R}. \quad (16b)$$

### 3.2. Dynamic solution

Substituting Eq. (6) into Eqs. (7a)–(7c) with  $R$  replaced by  $R^*$ , introducing non-dimensional displacement components  $\tilde{v} = v/R$  and  $\tilde{w} = w/R$ , and letting

$$\tilde{v}(\theta, t) = \bar{V}(\theta) e^{i\omega t}, \quad \tilde{w}(\theta, t) = \bar{W}(\theta) e^{i\omega t} \quad \text{and} \quad \psi(\theta, t) = \Psi(\theta) e^{i\omega t}, \quad (17)$$

in which  $\omega$  is the natural frequency, yields the following equations in terms of vibratory displacement components:

$$\frac{\partial^2 \bar{V}}{\partial \theta^2} + \alpha_1 \frac{\partial \bar{V}}{\partial \theta} + \alpha_2 \bar{V} + \alpha_3 \frac{\partial \bar{W}}{\partial \theta} + \alpha_4 \bar{W} + \alpha_5 \frac{\partial^2 \Psi}{\partial \theta^2} + \alpha_6 \frac{\partial \Psi}{\partial \theta} + \alpha_7 \Psi = 0, \quad (18a)$$

$$\frac{\partial^2 \bar{W}}{\partial \theta^2} + \beta_1 \frac{\partial \bar{W}}{\partial \theta} + \beta_2 \bar{W} + \beta_3 \frac{\partial \bar{V}}{\partial \theta} + \beta_4 \bar{V} + \beta_5 \frac{\partial \Psi}{\partial \theta} + \beta_6 \Psi = 0, \quad (18b)$$

$$\frac{\partial^2 \Psi}{\partial \theta^2} + \gamma_1 \frac{\partial \Psi}{\partial \theta} + \gamma_2 \Psi + \gamma_3 \frac{\partial^2 \bar{V}}{\partial \theta^2} + \gamma_4 \frac{\partial \bar{V}}{\partial \theta} + \gamma_5 \bar{V} + \gamma_6 \frac{\partial \bar{W}}{\partial \theta} + \gamma_7 \bar{W} = 0, \quad (18c)$$

where

$$\begin{aligned} \alpha_1 &= \frac{1}{\xi} \frac{\partial \xi}{\partial \theta} + \left( \frac{1}{EA + N^{(0)}} \right) \frac{\partial N^{(0)}}{\partial \theta}, & \alpha_2 &= \frac{-N^{(0)} - kGA}{\xi^2 \bar{R}^2 (EA + N^{(0)})} + \frac{R^2 \omega^2 \rho A}{\xi^2 (EA + N^{(0)})}, \\ \alpha_3 &= \frac{EA + kGA + 2N^{(0)}}{\xi \bar{R} (EA + N^{(0)})}, & \alpha_4 &= -\frac{1}{\xi \bar{R}^2} \frac{\partial \bar{R}}{\partial \theta} + \frac{\frac{\partial N^{(0)}}{\partial \theta}}{\xi \bar{R} (EA + N^{(0)})}, & \alpha_5 &= \frac{M^{(0)}}{R(EA + N^{(0)})}, \\ \alpha_6 &= \frac{1}{\xi R (EA + N^{(0)})} \left( \xi \frac{\partial M^{(0)}}{\partial \theta} - RQ^{(0)} + \frac{\partial \xi}{\partial \theta} M^{(0)} \right), \\ \alpha_7 &= \frac{1}{\xi \bar{R} (EA + N^{(0)})} \left( -\bar{R} \frac{\partial Q^{(0)}}{\partial \theta} - \frac{kGA}{\xi} - \frac{M^{(0)}}{\xi \bar{R} R} \right), & \beta_1 &= \frac{1}{\xi} \frac{\partial \xi}{\partial \theta} + \left( \frac{1}{\kappa GA + N^{(0)}} \right) \frac{\partial N^{(0)}}{\partial \theta}, \\ \beta_2 &= \frac{(-N^{(0)} - EA)}{\xi^2 \bar{R}^2 (kGA + N^{(0)})} + \frac{R^2 \omega^2 \rho A}{\xi^2 (kGA + N^{(0)})}, & \beta_3 &= -\frac{EA + kGA + 2N^{(0)}}{\xi \bar{R} (\kappa GA + N^{(0)})}, \\ \beta_4 &= \frac{1}{\xi \bar{R}^2} \frac{\partial \bar{R}}{\partial \theta} - \frac{1}{\xi \bar{R} (kGA + N^{(0)})} \left( \frac{\partial N^{(0)}}{\partial \theta} \right), & \beta_5 &= \frac{-1}{\xi (kGA + N^{(0)})} \left( kGA + \frac{2M^{(0)}}{\bar{R} R} \right), \\ \beta_6 &= \frac{1}{\xi \bar{R} R (\kappa GA + N^{(0)})} \left( -\frac{\partial M^{(0)}}{\partial \theta} + \frac{\partial \bar{R}}{\partial \theta} \frac{M^{(0)}}{\bar{R}} + \frac{R}{\xi} Q^{(0)} \right), & \gamma_1 &= \frac{1}{\xi} \frac{\partial \xi}{\partial \theta} + \frac{1}{EI + P^{(0)}} \left( \frac{\partial P^{(0)}}{\partial \theta} \right), \\ \gamma_2 &= \frac{1}{\xi^2 (EI + P^{(0)})} \left( -\frac{P^{(0)}}{\bar{R}^2} - R^2 kGA + \xi R \frac{\partial T^{(0)}}{\partial \theta} + R^2 \omega^2 \rho I \right), & \gamma_3 &= \frac{RM^{(0)}}{EI + P^{(0)}}, \\ \gamma_4 &= \frac{R \left( \xi \frac{\partial M^{(0)}}{\partial \theta} + RQ^{(0)} + \frac{\partial \xi}{\partial \theta} M^{(0)} \right)}{\xi (EI + P^{(0)})}, & \gamma_5 &= \frac{-R^2 \bar{R} kGA - \bar{R} M^{(0)}}{\xi^2 \bar{R}^2 (EI + P^{(0)})}, \\ \gamma_6 &= \frac{R^2 \bar{R} kGA + 2RM^{(0)}}{\xi \bar{R} (EI + P^{(0)})}, & \gamma_7 &= \frac{1}{\xi \bar{R} (EI + P^{(0)})} \left( R \frac{\partial M^{(0)}}{\partial \theta} + \frac{R^2 Q^{(0)}}{\xi} - \frac{RM^{(0)}}{\bar{R}} \frac{\partial \bar{R}}{\partial \theta} \right). \end{aligned} \quad (19)$$

In Eq. (19),  $\bar{R} = R^*/R$  and  $\xi = R \frac{\partial \theta}{\partial s}$ . Equations (18a)–(18c) are a set of ordinary differential equations with variable coefficients. The Frobenius method yields an analytical solution of these equations.

To construct a series solution to Eqs. (18a)–(18c), one has to express each variable coefficient as a Taylor series about a point on the arch,  $\eta$ . The variable coefficients are simply expressed as,



$$\begin{aligned}
 \alpha_1 &= \sum_{k=0}^K \bar{A}_k(\theta - \eta)^k, & \alpha_2 &= \sum_{k=0}^K \bar{B}_k(\theta - \eta)^k, & \alpha_3 &= \sum_{k=0}^K \bar{C}_k(\theta - \eta)^k, \\
 \alpha_4 &= \sum_{k=0}^K \bar{D}_k(\theta - \eta)^k, & \alpha_5 &= \sum_{k=0}^K \bar{E}_k(\theta - \eta)^k, & \alpha_6 &= \sum_{k=0}^K \bar{F}_k(\theta - \eta)^k, & \alpha_7 &= \sum_{k=0}^K \bar{G}_k(\theta - \eta)^k, \\
 \beta_1 &= \sum_{k=0}^K \hat{A}_k(\theta - \eta)^k, & \beta_2 &= \sum_{k=0}^K \hat{B}_k(\theta - \eta)^k, & \beta_3 &= \sum_{k=0}^K \hat{C}_k(\theta - \eta)^k, \\
 \beta_4 &= \sum_{k=0}^K \hat{D}_k(\theta - \eta)^k, & \beta_5 &= \sum_{k=0}^K \hat{E}_k(\theta - \eta)^k, & \beta_6 &= \sum_{k=0}^K \hat{F}_k(\theta - \eta)^k, \\
 \gamma_1 &= \sum_{k=0}^K \tilde{A}_k(\theta - \eta)^k, & \gamma_2 &= \sum_{k=0}^K \tilde{B}_k(\theta - \eta)^k, & \gamma_3 &= \sum_{k=0}^K \tilde{C}_k(\theta - \eta)^k, & \gamma_4 &= \sum_{k=0}^K \tilde{D}_k(\theta - \eta)^k, \\
 \gamma_5 &= \sum_{k=0}^K \tilde{E}_k(\theta - \eta)^k, & \gamma_6 &= \sum_{k=0}^K \tilde{F}_k(\theta - \eta)^k, & \gamma_7 &= \sum_{k=0}^K \tilde{G}_k(\theta - \eta)^k.
 \end{aligned}
 \tag{20}$$

Once the static stress resultants have been determined as described in the preceding section, the coefficients in Eq. (20) are obtained using the commercial symbolic logic computer package, Mathematica. Consequently, the solution of Eqs. (18a)–(18c) is,

$$\bar{V} = \sum_{j=0}^J A_j(\theta - \eta)^j, \quad \bar{W} = \sum_{j=0}^J B_j(\theta - \eta)^j, \quad \text{and} \quad \Psi = \sum_{j=0}^J D_j(\theta - \eta)^j.
 \tag{21}$$

Substituting Eqs. (20) and (21) into Eqs. (18a)–(18c) with careful arrangement and satisfying Eqs. (18a)–(18c) yield the following recursive formulae among coefficients  $A_i$ ,  $B_i$  and  $D_i$ .

$$\begin{aligned}
 A_{i+2} &= \frac{-1}{(i+1)(i+2)} \left\{ \sum_{k=0}^i [(k+1)\bar{A}_{i-k}A_{k+1} + \bar{B}_{i-k}A_k + (k+1)\bar{C}_{i-k}B_{k+1} + \bar{D}_{i-k}B_k \right. \\
 &\quad \left. + (k+1)(k+2)\bar{E}_{i-k}D_{k+2} + (k+1)\bar{F}_{i-k}D_{k+1} + \bar{G}_{i-k}D_k] \right\},
 \end{aligned}
 \tag{22a}$$

$$\begin{aligned}
 B_{i+2} &= \frac{-1}{(i+1)(i+2)} \left\{ \sum_{k=0}^i [(k+1)\hat{A}_{i-k}B_{k+1} + \hat{B}_{i-k}B_k + (k+1)\hat{C}_{i-k}A_{k+1} + \hat{D}_{i-k}A_k \right. \\
 &\quad \left. + (k+1)\hat{E}_{i-k}D_{k+1} + \hat{F}_{i-k}D_k] \right\},
 \end{aligned}
 \tag{22b}$$

$$\begin{aligned}
 D_{i+2} &= \frac{-1}{(i+1)(i+2)} \left\{ \sum_{k=0}^i [(k+1)\tilde{A}_{i-k}D_{k+1} + \tilde{B}_{i-k}D_k + (k+1)(k+2)\tilde{C}_{i-k}A_{k+2} \right. \\
 &\quad \left. + (k+1)\tilde{D}_{i-k}A_{k+1} + \tilde{E}_{i-k}A_k + (k+1)\tilde{F}_{i-k}B_{k+1} + \tilde{G}_{i-k}B_k] \right\},
 \end{aligned}
 \tag{22c}$$

where  $i = 0, 1, 2, \dots$ . Notably, the coefficients  $A_0, A_1, B_0, B_1, D_0$  and  $D_1$  are to be determined from the boundary conditions. As a result, the solution can be simply represented as,

$$\begin{Bmatrix} \bar{V}(\theta) \\ \bar{W}(\theta) \\ \Psi(\theta) \end{Bmatrix} = [S] \begin{Bmatrix} A_0 \\ A_1 \\ B_0 \\ B_1 \\ D_0 \\ D_1 \end{Bmatrix}, \tag{23}$$

where

$$[S] = \begin{bmatrix} \bar{v}_0(\theta) & \bar{v}_1(\theta) & \bar{v}_2(\theta) & \bar{v}_3(\theta) & \bar{v}_4(\theta) & \bar{v}_5(\theta) \\ \bar{w}_0(\theta) & \bar{w}_1(\theta) & \bar{w}_2(\theta) & \bar{w}_3(\theta) & \bar{w}_4(\theta) & \bar{w}_5(\theta) \\ \psi_0(\theta) & \psi_1(\theta) & \psi_2(\theta) & \psi_3(\theta) & \psi_4(\theta) & \psi_5(\theta) \end{bmatrix}, \tag{24}$$

and  $\bar{v}_j, \bar{w}_j,$  and  $\psi_j$  ( $j = 0, 1, 2, \dots, 5$ ) are polynomials whose coefficients are determined from Eq. (22).

Theoretically, Eqs. (23) and (24) can be used to determine the natural frequencies  $\omega$ , satisfying the prescribed boundary conditions. Sufficiently large  $K$  and  $J$  must be used in Eqs. (20) and (21), respectively, to yield accurate results. However, determining the coefficients in Eq. (20) for high orders of  $(\theta - \eta)$  is very difficult. Moreover, using very high order polynomials in Eq. (21) typically causes numerical difficulties. The convergence problem concerning the series solution also arises when the convergence radius of the solution can not cover the entire range of under consideration.

The dynamic stiffness matrix approach is introduced into the method of the series solution to overcome the above difficulties. As in a finite element approach, the arch under consideration is decomposed into numerous arch elements. The end displacements of the  $n$ th element (see Fig. 2) are determined from Eqs. (23) and (24) and expressed as,

$$\begin{Bmatrix} \bar{V}_n \\ \bar{W}_n \\ \Psi_n \\ \bar{V}_{n+1} \\ \bar{W}_{n+1} \\ \Psi_{n+1} \end{Bmatrix} = [\beta]_n \begin{Bmatrix} A_0 \\ A_1 \\ B_0 \\ B_1 \\ D_0 \\ D_1 \end{Bmatrix}_n, \tag{25}$$

where  $[\beta]_n$  is specified in Appendix A. Then, combining Eqs. (23)–(25) yields,

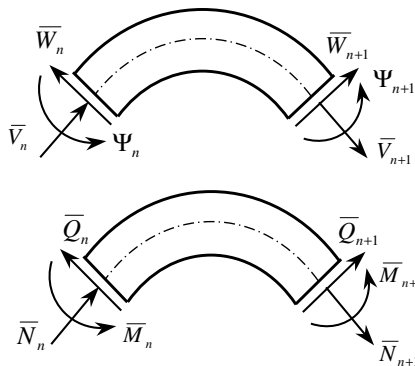


Fig. 2. Element of arch member with sign convention.

$$\begin{Bmatrix} \bar{V}(\theta) \\ \bar{W}(\theta) \\ \Psi(\theta) \end{Bmatrix} = [\bar{S}]_n \begin{Bmatrix} \bar{V}_n \\ \bar{W}_n \\ \Psi_n \\ \bar{V}_{n+1} \\ \bar{W}_{n+1} \\ \Psi_{n+1} \end{Bmatrix}, \tag{26}$$

where  $[\bar{S}]_n = [S][\beta]_n^{-1}$  is a matrix that is comprised of frequency dependent shape functions for the  $n$ th element.

As for Eq. (17), let

$$N(\theta, t) = \bar{N}(\theta)e^{i\omega t}, \quad Q(\theta, t) = \bar{Q}(\theta)e^{i\omega t}, \quad \text{and} \quad M(\theta, t) = \bar{M}(\theta)e^{i\omega t}. \tag{27}$$

From the relationship between the stress resultants and the displacement components, the end vibratory stress resultants of the  $n$ th element (see Fig. 2) are expressed in terms of end vibratory displacement components as,

$$\begin{Bmatrix} \bar{N}_n \\ \bar{Q}_n \\ \bar{M}_n \\ \bar{N}_{n+1} \\ \bar{Q}_{n+1} \\ \bar{M}_{n+1} \end{Bmatrix} = [K]_n \begin{Bmatrix} \bar{V}_n \\ \bar{W}_n \\ \Psi_n \\ \bar{V}_{n+1} \\ \bar{W}_{n+1} \\ \Psi_{n+1} \end{Bmatrix}, \tag{28}$$

where  $[K]_n = [\alpha]_n[\beta]_n^{-1}$  is the dynamic stiffness matrix for the  $n$ th arch element, and  $[\alpha]_n$  is also elucidated in Appendix A.

The continuity conditions of the end displacement components and the stress resultants between the adjacent elements assemble the relations in Eq. (28) for each element to form

$$[K]\{U\} = \{F\}, \tag{29}$$

where  $[K]$  represents the assemblage of the dynamic stiffness matrices of all elements and is called the global dynamic stiffness matrix of the whole arch;  $\{U\}$  is the vector of the end displacement components of elements, and  $\{F\}$  is a vector having non-zero unknown stress resultants at the end points on boundary. Eq. (29) can be further rewritten as,

$$\begin{bmatrix} [K_{uu}] & [K_{ub}] \\ [K_{bu}] & [K_{bb}] \end{bmatrix} \begin{Bmatrix} \{U_u\} \\ \{U_b\} \end{Bmatrix} = \begin{Bmatrix} \{0\} \\ \{F_b\} \end{Bmatrix}, \tag{30}$$

where  $\{U_u\}$  corresponds to the unknown nodal displacement components;  $\{U_b\}$  are the prescribed displacement components at the boundaries, and  $\{F_b\}$  are the unknown stress resultants on the displacement prescribed boundaries. The natural frequencies of the arch are  $\omega$ 's that yield a zero determinant of  $[K_{uu}]$ , since  $\{U_b\}$  vanishes in a free vibration problem.

The use of shear deformable theory with initial shape (SDTIS) to find the vibration frequencies of a loaded circular arch requires only that  $R^*$  be replaced by  $R$ , a constant, and that  $\xi = 1$  and  $\bar{R} = 1$  are set in the foregoing formulations. The terms involving the derivatives of  $\bar{R}$  and  $\xi$  with respect to  $\theta$  should vanish.

#### 4. Numerical results for vibration frequencies

##### 4.1. Convergence studies

The solution for the vibration frequencies of an arch developed above must converge as the number of elements or the number of terms in Eqs. (20) and (21) increases to obtain accurate results. Table 1 summarizes the results of a convergence study of non-dimensional vibration frequencies for two clamped circular arches under no load. The arches have  $h/R = 0.01$  and opening angles of  $\theta_0 = 100^\circ$  and  $\theta_0 = 1$  rad, respectively. Notably, all the numerical results presented in this paper pertain to circular arches with rectangular cross-sections and a Poisson's ratio of 0.3. Rapid convergence of the non-dimensional frequency parameters,  $\lambda = \omega R^2(\rho A/EI)^{1/2}$ , to the exact values as the number of elements increases or the number of series solution terms ( $J + 1$ ) in Eq. (21) increases supports the validity of the proposed solution. The results of Tseng et al. (1997) shown in Table 1 were obtained from an exact solution for a shear-deformable arch, while the results of Qatu (1993b) were obtained from the Ritz method and neglecting the effects of shear deformation.

Table 2 presents the convergence of non-dimensional frequency parameters  $\lambda$  for a clamped arch with  $h/R = 0.02$  and  $\theta_0 = 40^\circ$ , subjected to uniformly distributed vertical loading,  $\gamma$ , that makes the non-dimensional loading parameter  $\beta (= \gamma R^3/EI)$  equal to 100. The results were obtained based on the shear deformable theory with deformed state. As expected, an accurate solution can be obtained either by increasing the number of elements or by increasing the values of both  $K$  and  $J$  in Eqs. (20) and (21), respectively. Fewer elements must cooperate with greater values of  $K$  and  $J$  to produce accurate results. For a specified number of elements, the results may converge to true values in an oscillatory fashion as the values of  $K$  and  $J$  increase.

Table 1  
Convergence of non-dimensional frequency parameters  $\lambda$  for two unloaded, clamped arches with  $h/R = 0.01$

$\theta_0$	Present solution						Published results
	Element no.	Modes	Solution terms ( $J + 1$ )				
			5	10	15	20	
100°	4	1	44.921	17.919	17.916	17.916	17.916*
		2	250.17	34.724	34.643	34.643	34.643*
		3	292.29	62.970	62.789	62.789	62.789*
		4	601.23	96.381	92.677	92.677	92.677*
	8	1	18.736	17.916	17.916	17.916	
		2	35.632	34.643	34.643	34.643	
		3	63.419	62.790	62.789	62.789	
		4	91.103	92.685	92.677	92.677	
1 rad	2	1	30.747	59.289	59.066	59.066	59.159**
		2	173.87	199.05	107.57	107.55	107.85**
		3	347.30	293.96	196.06	196.06	196.98**
		4	1063.9	303.36	268.46	267.04	268.54**
	4	1	63.860	59.066	59.066	59.066	
		2	203.84	107.63	107.55	107.55	
		3	347.90	196.23	196.06	196.06	
		4	397.60	269.29	267.26	267.26	

Note: \*denotes the results of Tseng et al. (1997); \*\*denotes the results of Qatu (1993b).

Table 2

Convergence of non-dimensional frequency parameters  $\lambda$  for a clamped arch with  $h/R = 0.02$  and  $\theta_0 = 40^\circ$  under statically vertical loading  $\beta = 100$

Element no.	Mode no.	$(K + 1)$ in Eq. (20)	Solution terms $(J + 1)$ in Eq. (21)			
			5	10	15	20
3	1	2	110.98	83.447	83.342	83.342
		4	111.17	83.115	83.065	83.065
		6	111.17	83.160	83.120	83.120
	2	2	248.58	110.64	110.66	110.66
		4	248.60	110.86	110.85	110.85
		6	248.60	110.85	110.84	110.84
	3	2	461.33	223.10	222.93	222.93
		4	461.39	222.85	222.71	222.71
		6	461.39	222.87	222.72	222.72
	4	2	1237.7	354.20	352.52	352.52
		4	1237.8	354.15	352.46	352.46
		6	1237.8	354.13	352.45	352.45
6	1	2	93.451	83.121	83.121	83.121
		4	93.742	83.118	83.118	83.118
		6	93.742	83.119	83.118	83.118
	2	2	116.25	110.85	110.85	110.85
		4	116.09	110.84	110.84	110.84
		6	116.09	110.84	110.84	110.84
	3	2	245.03	222.71	222.71	222.71
		4	245.17	222.72	222.72	222.72
		6	245.17	222.72	222.72	222.72
	4	2	398.33	352.41	352.41	352.41
		4	398.52	352.46	352.45	352.45
		6	398.52	352.46	352.45	352.45

4.2. Results and discussion

This section provides numerical results on the vibration frequencies of clamped arches with various opening angles, under uniform vertical static loads. Problems of symmetry are analyzed herein. Various theories were applied to determine the vibration frequencies. To ensure results with high accuracy, the numerical results were obtained by decomposing an arch into eight equal-length elements and using  $K = 12$  and  $J = 19$  in Eqs. (20) and (21), respectively, for each element.

Figs. 3–5 plot the variation of  $\lambda$  with  $\beta$  for arches with  $h/R = 0.1$  and  $\theta_0 = 40^\circ, 80^\circ$  and  $120^\circ$ , respectively. Figs. 6 and 7 plot the results for arches with  $h/R = 0.02$  and  $\theta_0 = 40^\circ$  and  $80^\circ$ , respectively. Three theories were applied to determine the frequencies – shear deformable theory with deformed state (SDTDS), shear deformable theory with initial shape (SDTIS), and classical theory neglecting shear deformation (CTNSD). The results yielded by the classical theory were obtained by implementing the formulation of Huang and Nieh (2002), who used a series solution along with the dynamic stiffness matrix approach to solve Eqs. (11a) and (11b). In the legend of these figures, the stress resultants inside parentheses are those considered in Eqs. (7a)–(7c), while  $A_i$  and  $S_i$  represent the  $i$ th anti-symmetric and symmetric modes, respectively. (All) labels the results obtained by considering all the stress resultants in Eqs. (7a)–(7c). Notably, the range of  $\beta$  for Figs. 3–5 was determined from the static strain  $\varepsilon_{\theta\theta}^{(L)}$  at  $z = h/2$ , shown in Fig. 8. Fig. 8 implies that most

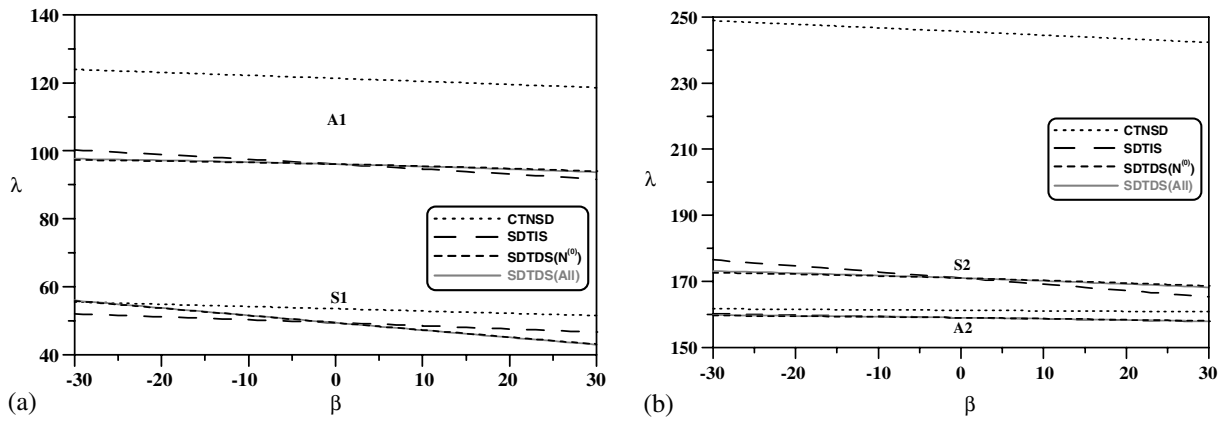


Fig. 3.  $\lambda$  versus  $\beta$  for the arch having  $h/R = 0.1$  and  $\theta_0 = 40^\circ$  based on different theories: (a) for first symmetric and anti-symmetric modes, (b) for second symmetric and anti-symmetric modes.

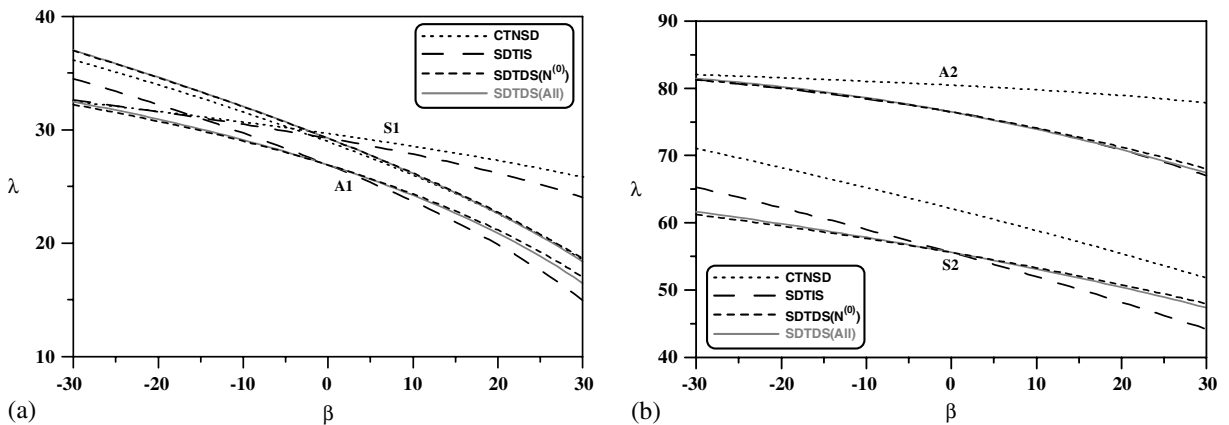


Fig. 4.  $\lambda$  versus  $\beta$  for the arch having  $h/R = 0.1$  and  $\theta_0 = 80^\circ$  based on different theories: (a) for first symmetric and anti-symmetric modes, (b) for second symmetric and anti-symmetric modes.

parts of the arches considered in Figs. 3–5 may yield when  $\beta > 30$ . The range of  $\beta$  in Figs. 6 and 7 was selected such that the values of  $\beta$  were less than the lowest buckling loads for the arches considered in these two figures. The buckling loads will be presented in Section 5.2.

The results shown in Figs. 3–7 support various conclusions:

- (a) The results based on shear deformable theory indicate that among the initial stress resultants,  $N^{(0)}$  has the most significant effect on the vibration frequencies in the ranges of  $\beta$  considered.
- (b) Comparing the results obtained from shear deformable theory with deformed state with those obtained from shear deformable theory with initial shape indicates that, as expected, static deformation more strongly affects vibration frequencies when  $\beta$  is larger. However, no certain trend in the effect of static deformations on vibration frequency is evident. The static deformations may increase or reduce the frequencies, depending on the geometric properties of the arch under consideration, the sign of  $\beta$ , and the considered mode.

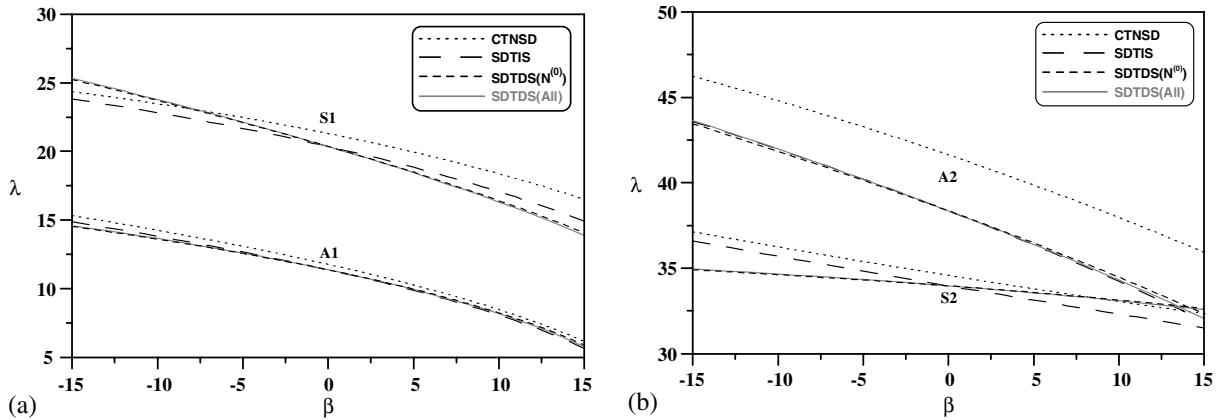


Fig. 5.  $\lambda$  versus  $\beta$  for the arch having  $h/R = 0.1$  and  $\theta_0 = 120^\circ$  based on different theories: (a) for first symmetric and anti-symmetric modes, (b) for second symmetric and anti-symmetric modes.

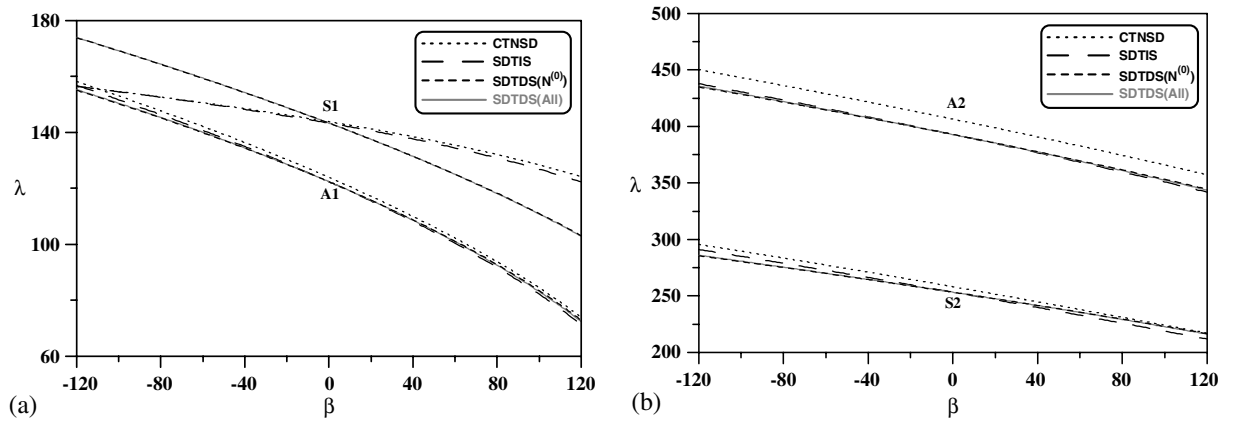


Fig. 6.  $\lambda$  versus  $\beta$  for the arch having  $h/R = 0.02$  and  $\theta_0 = 40^\circ$  based on different theories: (a) for first symmetric and anti-symmetric modes, (b) for second symmetric and anti-symmetric modes.

(c) Comparison of the results based on shear deformable theory with initial shape with those obtained by classical theory neglecting shear deformation reveals that neglecting the effects of shear deformation generally increases the vibration frequencies, especially for the arches with small  $\theta_0$  and large  $h/R$ , or for higher modes. The relative differences between the frequencies obtained according to these two theories may increase as positive  $\beta$  is getting large.

### 5. Numerical results for buckling loads

The buckling loads determined from the equations governing the vibrations of a statically loaded arch, such as Eqs. (7a)–(7c), are those loads that make the vibration frequencies vanish (Wasserman, 1977). In finding a buckling load, prebuckling deformations are frequently assumed to be small and neglected. Hence, the shear deformation theory with initial shape and the classical theory neglecting shear

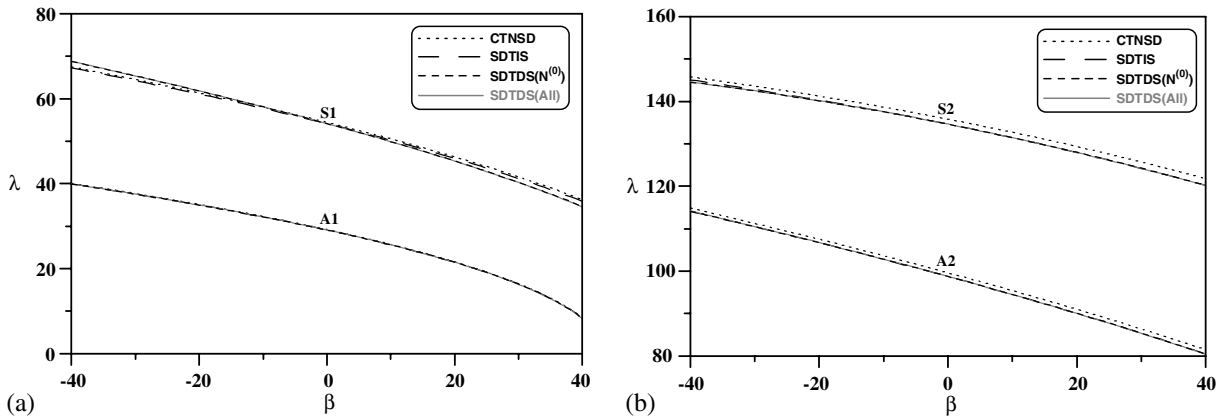


Fig. 7.  $\lambda$  versus  $\beta$  for the arch having  $h/R = 0.02$  and  $\theta_0 = 80^\circ$  based on different theories: (a) for first symmetric and anti-symmetric modes, (b) for second symmetric and anti-symmetric modes.

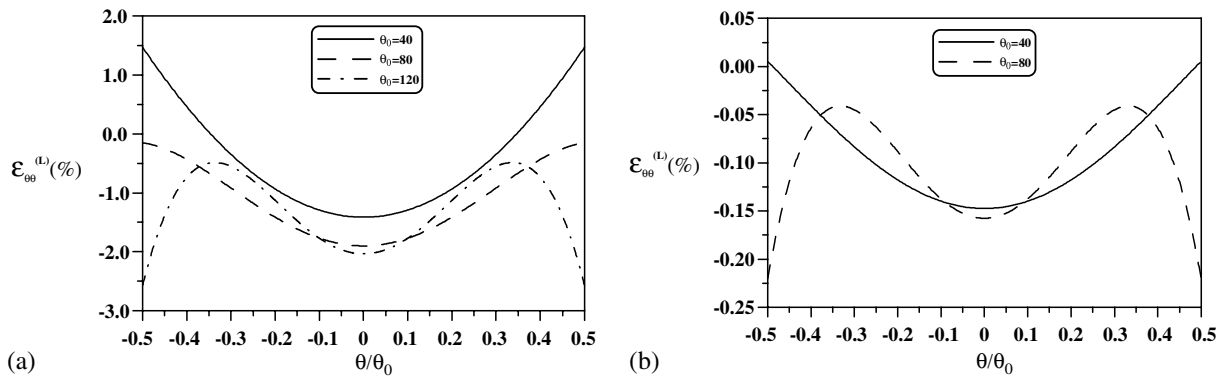


Fig. 8. The distribution of static  $\epsilon_{\theta\theta}^{(L)}$ : (a) for  $h/R = 0.1$  and  $\beta = 15$ , (b) for  $h/R = 0.02$  and  $\beta = 30$ .

deformation will be applied to determine the buckling loads, and the results of these two theories will be compared.

### 5.1. Convergence studies

Consider a fixed circular arch with  $\theta_0 = 180^\circ$  and  $h/R = 0.01$ , under a constant directional uniform pressure that remains normal to the undeformed axis of the arch. The procedure given in Section 3.1 can be followed to find the static stress resultants presented in Appendix B.

Table 3 lists the convergence of non-dimensional buckling loads obtained by applying shear deformable theory with initial shape and compares the results with those published results obtained by neglecting shear deformation effects. Notably, Wempner and Kesti (1962) formulated their governing equation based on a static approach, and solved it analytically, while Chidamparam (1993) used a perturbation technique to derive the governing equations for buckling loads and solved them by the Ritz method. Since the distributions of stress resultants are almost uniform for the arch considered here, increasing  $K$  in Eq. (20) does not significantly affect the results. As expected, the effects of shear deformation on buckling loads are not



Table 3

Convergence of non-dimensional buckling loads  $\beta$  for a fixed circular arch with  $\theta_0 = 180^\circ$  and  $h/R = 0.01$  under a constant directional uniform pressure

	Element no.	$(K + 1)$ in Eq. (20)	Solution terms $(J + 1)$ in Eq. (21)			Published results
			10	15	20	
Lowest buckling load	2	1	18.470	9.0035	8.9975	9.00*
		3	18.470	9.0035	8.9975	9.0003**
	4	1	9.0737	8.9975	8.9975	
		3	9.0738	8.9975	8.9975	
Second buckling load	2	1	39.701	14.559	14.271	14.279**
		3	39.701	14.559	14.271	
	4	1	15.339	14.271	14.271	
		3	15.339	14.271	14.271	

Note: \*denotes the results of Wempner and Kesti (1962); \*\*denotes the results of Chidamparam (1993).

significant for a long and thin arch, so the convergent results obtained by the present approach agree excellently with the published results, supporting the validity of the present approach.

5.2. Results and discussion

Figs. 9 and 10 plot the buckling loads as a function of opening angle for clamped arches with  $h/R = 0.1$  and  $0.02$ , respectively, under uniform gravity loading. In the figures, S1 and A1 represent the buckling loads that correspond to the first symmetric and anti-symmetric modes, respectively. The buckling loads were computed based on classical theory neglecting shear deformation (CTNSD) and shear deformable theory (SDTIS) along with considering all initial stress resultants or  $N^{(0)}$  only. The numerical results were obtained by decomposing an arch into eight elements of equal length and using  $K = 12$  and  $J = 19$  in Eqs. (20) and (21), respectively, for each element. The results of the classical theory were obtained using the formulations given in Huang and Nieh (2002) and Nieh et al. (2003).

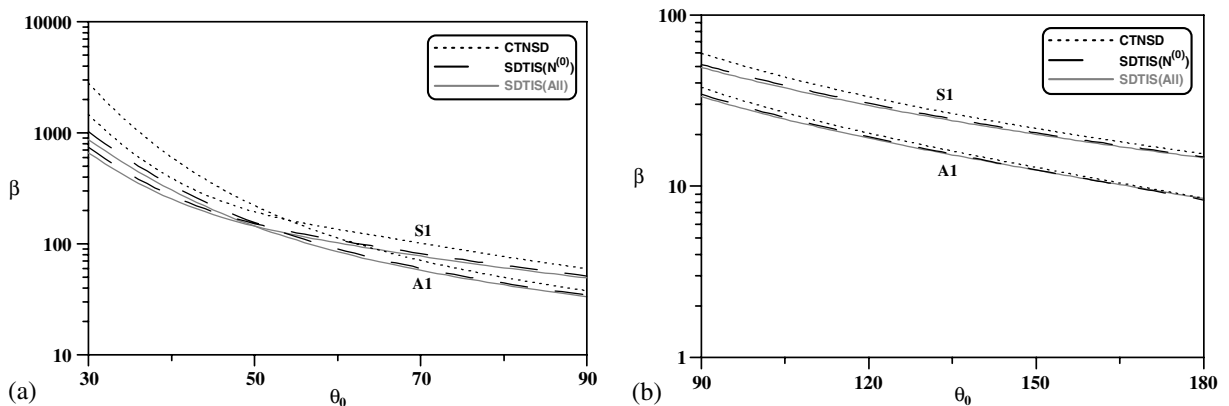


Fig. 9. Variation of buckling loads with  $\theta_0$  for arches with  $h/R = 0.1$ : (a) for  $30^\circ \leq \theta_0 \leq 90^\circ$ , (b) for  $90^\circ \leq \theta_0 \leq 180^\circ$ .

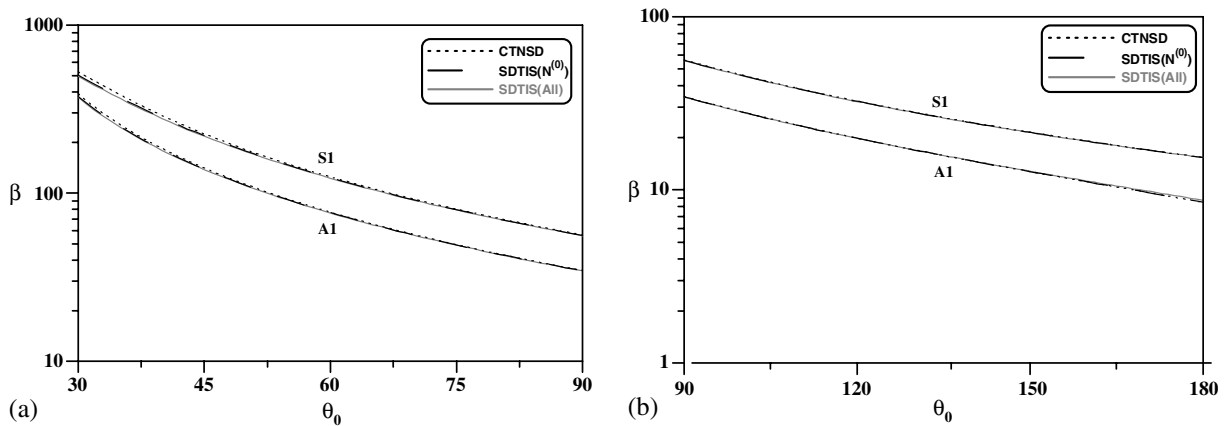


Fig. 10. Variation of buckling loads with  $\theta_0$  for arches with  $h/R = 0.02$ : (a) for  $30^\circ \leq \theta_0 \leq 90^\circ$ , (b) for  $90^\circ \leq \theta_0 \leq 180^\circ$ .

Fig. 9 shows that for  $\theta_0$  between  $30^\circ$  and  $180^\circ$ , the lowest buckling loads for arches with  $h/R = 0.1$  correspond to symmetric modes when  $\theta_0$  is below around  $50^\circ$ , above which they correspond to anti-symmetric modes. The differences between the buckling loads obtained by considering all the static stress resultants and those obtained by considering only  $N^{(0)}$  generally become more significant as  $\theta_0$  declines. For a given  $\theta_0$ , the differences between the second buckling loads exceed those between the lowest buckling loads. Comparing the results of shear deformable theory with the results obtained by classical theory reveals that neglecting the effects of shear deformation leads to considerably larger buckling loads, especially for small  $\theta_0$ . Notably, the strain distributions in Fig. 8 imply that the arches with small  $\theta_0$  may yield before buckling.

Fig. 10 indicates that the lowest buckling loads for  $h/R = 0.02$  correspond to anti-symmetric modes. Among the initial stress resultants,  $N^{(0)}$  dominates the lowest and second buckling loads. Shear deformations do not significantly affect the buckling loads.

## 6. Concluding remarks

By applying a variational principle for dynamic problems concerning an elastic body under initial stresses, this work has derived the first known equations governing vibrations of preloaded circular arches that are shear-deformable. The proposed governing equations account for the effects of the stress resultants— $N^{(0)}$ ,  $Q^{(0)}$ ,  $M^{(0)}$ ,  $P^{(0)}$  and  $T^{(0)}$ —due to static preloading. The effects of the static deformations on the vibrations can also be included. Although the proposed governing equations are more complex than currently available equations that ignore shear deformation, they can be easily solved.

An analytical solution to the proposed governing equations was developed to analyze the free vibration and stability of a circular arch under uniformly distributed vertical loading. The static solution for the arch under vertical loading was determined in closed form. Then, vibration frequencies or buckling loads were determined by the dynamic stiffness matrix approach combined with series solutions. The solution was validated by comparing present convergence results with the published data on the vibration frequencies of a unloaded circular arch and on the buckling loads of a circular arch under a constant directional uniform pressure.

This study also presents the vibration frequencies and buckling loads for clamped arches with rectangular cross-sections,  $h/R = 0.02$  or  $0.1$ , and various opening angles. These results are compared to those

published, obtained by neglecting shear deformation. The comparison reveals that shear deformation markedly affects the vibration frequencies for thick ( $h/R = 0.1$ ) arches or for higher modes. Shear deformations do not significantly affect the lowest and second buckling loads for arches with  $h/R = 0.02$ .

Traditionally,  $N^{(0)}$  is considered primarily to affect the vibration frequencies and buckling loads of loaded arches. Among the static stress resultants,  $N^{(0)}$  is indeed the most important factor that influences the vibration frequencies over the ranges of static loading,  $\beta$ , considered herein. In contrast, this work shows that the buckling loads of thick and shallow arches obtained by considering only  $N^{(0)}$  in the proposed equations may differ substantially from those determined by considering all initial stress resultants.

Generally, the deformations caused by static loads may significantly affect the vibration behaviors of a loaded arch. For example, for the arch with  $h/R = 0.1$  and  $\theta_0 = 40^\circ$ , static deformations strongly affect the vibration frequencies for  $|\beta| \geq 10$ , which is far from the lowest buckling load for the arch. Furthermore, static deformations may increase or reduce vibration frequencies, depending on the geometric properties of the arch under consideration, the sign of  $\beta$ , and which mode is considered.

Although only the vibration frequencies and buckling loads were investigated here, the proposed solution can combine with Laplace transform (Huang et al., 2000) to determine the transient responses of preloaded circular arches. The solution can also be incorporated with Fourier transform to study stationary random vibrations of preloaded circular arches. In these cases, the responses of the dynamic stress resultants are accurately determined because the shape functions for the displacement components in each arch element follow from an analytical solution to the corresponding governing equations.

### Acknowledgement

The authors would like to thank the National Science Council of the Republic of China for financially supporting this research under contract no. NSC 90-2211-E-009-035.

### Appendix A. The expression of $[\beta]_n$ and $[\alpha]_n$

$$[\beta]_n = \begin{bmatrix} \bar{v}_0(\theta_n) & \bar{v}_1(\theta_n) & \bar{v}_2(\theta_n) & \bar{v}_3(\theta_n) & \bar{v}_4(\theta_n) & \bar{v}_5(\theta_n) \\ \bar{w}_0(\theta_n) & \bar{w}_1(\theta_n) & \bar{w}_2(\theta_n) & \bar{w}_3(\theta_n) & \bar{w}_4(\theta_n) & \bar{w}_5(\theta_n) \\ \psi_0(\theta_n) & \psi_1(\theta_n) & \psi_2(\theta_n) & \psi_3(\theta_n) & \psi_4(\theta_n) & \psi_5(\theta_n) \\ \bar{v}_0(\theta_{n+1}) & \bar{v}_1(\theta_{n+1}) & \bar{v}_2(\theta_{n+1}) & \bar{v}_3(\theta_{n+1}) & \bar{v}_4(\theta_{n+1}) & \bar{v}_5(\theta_{n+1}) \\ \bar{w}_0(\theta_{n+1}) & \bar{w}_1(\theta_{n+1}) & \bar{w}_2(\theta_{n+1}) & \bar{w}_3(\theta_{n+1}) & \bar{w}_4(\theta_{n+1}) & \bar{w}_5(\theta_{n+1}) \\ \psi_0(\theta_{n+1}) & \psi_1(\theta_{n+1}) & \psi_2(\theta_{n+1}) & \psi_3(\theta_{n+1}) & \psi_4(\theta_{n+1}) & \psi_5(\theta_{n+1}) \end{bmatrix}_n, \tag{A.1}$$

$$[\alpha]_n = [\alpha_1]_n + [\alpha_2]_n + [\alpha_3]_n, \tag{A.2}$$

$$[\alpha_1]_n = \begin{bmatrix} -\bar{k}_1 \bar{v}'_0(\theta_n) & -\bar{k}_1 \bar{v}'_1(\theta_n) & -\bar{k}_1 \bar{v}'_2(\theta_n) & -\bar{k}_1 \bar{v}'_3(\theta_n) & -\bar{k}_1 \bar{v}'_4(\theta_n) & -\bar{k}_1 \bar{v}'_5(\theta_n) \\ -\bar{k}_2 \bar{w}'_0(\theta_n) & -\bar{k}_2 \bar{w}'_1(\theta_n) & -\bar{k}_2 \bar{w}'_2(\theta_n) & -\bar{k}_2 \bar{w}'_3(\theta_n) & -\bar{k}_2 \bar{w}'_4(\theta_n) & -\bar{k}_2 \bar{w}'_5(\theta_n) \\ -\bar{k}_3 \psi'_0(\theta_n) & -\bar{k}_3 \psi'_1(\theta_n) & -\bar{k}_3 \psi'_2(\theta_n) & -\bar{k}_3 \psi'_3(\theta_n) & -\bar{k}_3 \psi'_4(\theta_n) & -\bar{k}_3 \psi'_5(\theta_n) \\ \tilde{k}_1 \bar{v}'_0(\theta_{n+1}) & \tilde{k}_1 \bar{v}'_1(\theta_{n+1}) & \tilde{k}_1 \bar{v}'_2(\theta_{n+1}) & \tilde{k}_1 \bar{v}'_3(\theta_{n+1}) & \tilde{k}_1 \bar{v}'_4(\theta_{n+1}) & \tilde{k}_1 \bar{v}'_5(\theta_{n+1}) \\ \tilde{k}_2 \bar{w}'_0(\theta_{n+1}) & \tilde{k}_2 \bar{w}'_1(\theta_{n+1}) & \tilde{k}_2 \bar{w}'_2(\theta_{n+1}) & \tilde{k}_2 \bar{w}'_3(\theta_{n+1}) & \tilde{k}_2 \bar{w}'_4(\theta_{n+1}) & \tilde{k}_2 \bar{w}'_5(\theta_{n+1}) \\ \tilde{k}_3 \psi'_0(\theta_{n+1}) & \tilde{k}_3 \psi'_1(\theta_{n+1}) & \tilde{k}_3 \psi'_2(\theta_{n+1}) & \tilde{k}_3 \psi'_3(\theta_{n+1}) & \tilde{k}_3 \psi'_4(\theta_{n+1}) & \tilde{k}_3 \psi'_5(\theta_{n+1}) \end{bmatrix}_n, \tag{A.3}$$

$$[\alpha_2]_n = \begin{bmatrix} -\hat{k}_1 \bar{w}_0(\theta_n) & -\hat{k}_1 \bar{w}_1(\theta_n) & -\hat{k}_1 \bar{w}_2(\theta_n) & -\hat{k}_1 \bar{w}_3(\theta_n) & -\hat{k}_1 \bar{w}_4(\theta_n) & -\hat{k}_1 \bar{w}_5(\theta_n) \\ \hat{k}_2 \bar{v}_0(\theta_n) & \hat{k}_2 \bar{v}_1(\theta_n) & \hat{k}_2 \bar{v}_2(\theta_n) & \hat{k}_2 \bar{v}_3(\theta_n) & \hat{k}_2 \bar{v}_4(\theta_n) & \hat{k}_2 \bar{v}_5(\theta_n) \\ 0 & 0 & 0 & 0 & 0 & 0 \\ \tilde{k}_1 \bar{w}_0(\theta_{n+1}) & \tilde{k}_1 \bar{w}_1(\theta_{n+1}) & \tilde{k}_1 \bar{w}_2(\theta_{n+1}) & \tilde{k}_1 \bar{w}_3(\theta_{n+1}) & \tilde{k}_1 \bar{w}_4(\theta_{n+1}) & \tilde{k}_1 \bar{w}_5(\theta_{n+1}) \\ -k_2 \bar{v}_0(\theta_{n+1}) & -k_2 \bar{v}_1(\theta_{n+1}) & -k_2 \bar{v}_2(\theta_{n+1}) & -k_2 \bar{v}_3(\theta_{n+1}) & -k_2 \bar{v}_4(\theta_{n+1}) & -k_2 \bar{v}_5(\theta_{n+1}) \\ 0 & 0 & 0 & 0 & 0 & 0 \end{bmatrix}_n, \quad (\text{A.4})$$

$$[\alpha_3]_n = EI \begin{bmatrix} 0 & 0 & 0 & 0 & 0 & 0 \\ \psi_0(\theta_n) & \psi_1(\theta_n) & \psi_2(\theta_n) & \psi_3(\theta_n) & \psi_4(\theta_n) & \psi_5(\theta_n) \\ 0 & 0 & 0 & 0 & 0 & 0 \\ 0 & 0 & 0 & 0 & 0 & 0 \\ -\psi_0(\theta_{n+1}) & -\psi_1(\theta_{n+1}) & -\psi_2(\theta_{n+1}) & -\psi_3(\theta_{n+1}) & -\psi_4(\theta_{n+1}) & -\psi_5(\theta_{n+1}) \\ 0 & 0 & 0 & 0 & 0 & 0 \end{bmatrix}_n, \quad (\text{A.5})$$

where  $\bar{k}_1 = EA\zeta(\theta_n)$ ,  $\bar{k}_2 = \kappa GA\zeta(\theta_n)$ ,  $\bar{k}_3 = EI\zeta(\theta_n)$ ,  $\tilde{k}_1 = EA\zeta(\theta_{n+1})$ ,  $\tilde{k}_2 = \kappa GA\zeta(\theta_{n+1})$ ,  $\tilde{k}_3 = EI\zeta(\theta_{n+1})$ ,  $\hat{k}_1 = EA/\bar{R}(\theta_n)$ ,  $\hat{k}_2 = \kappa GA/\bar{R}(\theta_n)$ ,  $k_1 = EA/\bar{R}(\theta_{n+1})$ , and  $k_2 = \kappa GA/\bar{R}(\theta_{n+1})$ . It should be noted that the superscript “ $\sim$ ” in Eq. (A.3) denotes the derivatives with respect to  $\theta$ .

## Appendix B. Initial equilibrium state of a circular arch under constant directional pressure

The equilibrium equations are

$$(N^{(0)})' + \frac{Q^{(0)}}{R} = 0, \quad (\text{B.1})$$

$$(Q^{(0)})' - \frac{N^{(0)}}{R} = \gamma, \quad (\text{B.2})$$

$$(M^{(0)})' + Q^{(0)} = 0. \quad (\text{B.3})$$

Through direct integration, one can obtain

$$Q^{(0)} = C_1 \cos \theta + C_2 \sin \theta, \quad (\text{B.4})$$

$$N^{(0)} = -C_1 \sin \theta + C_2 \cos \theta - R\gamma, \quad (\text{B.5})$$

$$M^{(0)} = -C_1 R \sin \theta + C_2 R \cos \theta + C_3, \quad (\text{B.6})$$

By substituting Eqs. (B.4)–(B.6) into the relations between displacement components and stress resultants and through direct integration again, one can obtain

$$v^{(0)} = -C_3 \frac{R^2 \theta}{EI} + C_4 \cos \theta + C_5 \sin \theta - C_6 R + \tilde{\delta}_1 \theta \cos \theta + \tilde{\delta}_2 \theta \sin \theta \quad (\text{B.7})$$

$$w^{(0)} = \left( -C_1 \frac{R}{EA} + C_4 - \tilde{\delta}_2 \right) \sin \theta + \left( C_2 \frac{R}{EA} - C_5 - \tilde{\delta}_1 \right) \cos \theta + C_3 \frac{R^2}{EI} - \tilde{\delta}_2 \theta \cos \theta + \tilde{\delta}_1 \theta \sin \theta - \frac{R^2 \gamma}{EA}, \quad (\text{B.8})$$

$$\psi^{(0)} = \frac{R}{EI} \{C_1 R \cos \theta + C_2 R \sin \theta + C_3 \theta\} + C_6, \quad (\text{B.9})$$

where

$$\tilde{\delta}_1 = \frac{R}{2E} \left( \frac{1}{A} + \frac{E}{\kappa GA} + \frac{R^2}{I} \right) C_2, \quad (\text{B.10})$$

$$\delta_2 = -\frac{R}{2E} \left( \frac{1}{A} + \frac{E}{\kappa GA} + \frac{R^2}{I} \right) C_1, \quad (\text{B.11})$$

Coefficients  $C_1 \sim C_6$  are also to be determined by the specified boundary conditions.

## References

- Chidamparam, P., 1993. Free vibration and buckling of curved beams subjected to distributed loads. Ph.D. Dissertation, The Ohio State University.
- Chidamparam, P., Leissa, A.W., 1993. Vibrations of planar curved beams, rings, and arches. *Applied Mechanics Reviews* 46 (9), 467–483.
- Chidamparam, P., Leissa, A.W., 1995. Influence of centerline extensibility on the in-plane free vibrations of loaded circular arches. *Journal of Sound and Vibration* 183 (5), 779–795.
- Gjelsvik, A., Bodner, S.R., 1962. Energy criterion and snap buckling of arches. *Journal of The Engineering Mechanics Division ASCE* 88 (EM5), 87–134.
- Huang, C.S., Tseng, Y.P., Leissa, A.W., Nieh, K.Y., 1998. An exact solution for in-plane vibration of an arch with variable curvature and cross-section. *International Journal of Mechanical Science* 40 (11), 1159–1173.
- Huang, C.S., Tseng, Y.P., Chang, S.H., Hung, C.L., 2000. Out-of-plane dynamic analysis of beams with arbitrarily varying curvature and cross-section by dynamic stiffness matrix method. *International Journal of Solids and Structures* 37, 495–513.
- Huang, C.S., Nieh, K.Y., 2002. An analytical solution for vibrations of loaded circular arches, *Proceedings of the 6th Structural Engineering, Ping-Tung, Taiwan* (in Chinese).
- Laura, P.A.A., Maurizi, M.J., 1987. Recent research on vibrations of arch-type structures. *The Shock and Vibration Digest* 19 (1), 6–9.
- Lin, J.L., Soedel, W., 1988. General in-plane vibrations of rotating thick and thin rings. *Journal of Sound and Vibration* 122, 547–570.
- Love, A.E.H., 1944. *A Treatise on the Mathematical Theory of Elasticity*, fourth ed. Dover, New York.
- Kang, K.J., Bert, C.W., Striz, A.G., 1996. Vibration and buckling analysis of circular arches using DQM. *Computers and Structures* 60 (1), 49–57.
- Kawakami, M., Sakiyama, T., Matsuda, H., Morita, C., 1995. In-plane and out-of plane free vibrations of curved beams with variable sections. *Journal of Sound and Vibration* 187 (3), 381–401.
- Markus, S., Nanasi, T., 1981. Vibration of curved beams. *The Shock and Vibration Digest* 13 (4), 3–14.
- Matsunaga, H., 1996. In-plane vibration and stability of shallow circular arches subjected to axial forces. *International Journal of Solids and Structures* 33 (4), 469–482.
- Nieh, K.Y., Huang, C.S., Tseng, I.P., 2003. An analytical solution for in-plane free vibration and stability of loaded elliptic arches. *Computers and Structures* 81 (13), 1311–1327.
- Oh, S.J., Lee, B.K., Lee, I.W., 1999. Natural frequencies of non-circular arches with rotatory inertia and shear deformation. *Journal of Sound and Vibration* 219 (1), 23–33.
- Perkins, N.C., 1990. Planar vibration of an elastica arch: theory and experiment. *Journal of Vibration and Acoustics* 112, 374–379.
- Plaut, R.H., Johnson, E.R., 1981. The effects of initial thrust and elastic foundation on the vibration frequencies of a shallow arch. *Journal of Sound and Vibration* 78 (4), 565–571.
- Qatu, M.S., 1993a. Theories and analysis of thin and moderately thick laminated composite curved beams. *International Journal of Solids and Structures* 30 (20), 2743–2756.
- Qatu, M.S., 1993b. Vibration of laminated composite arches with deep curvature and arbitrary boundaries. *Computers and Structures* 47 (2), 305–311.
- Schreyer, H.L., Masur, E.F., 1966. Buckling of shallow arches. *Journal of The Engineering Mechanics Division, ASCE* 92 (EM4), 1–17.
- Timoshenko, S., Gere, J.M., 1961. *Theory of Elastic Stability*. McGraw-Hill, New York.
- Tseng, Y.P., Huang, C.S., Lin, C.J., 1997. Dynamic stiffness analysis for in-plane vibrations of arches with variable curvature. *Journal of Sound and Vibration* 207 (1), 15–31.

- Tseng, Y.P., Huang, C.S., Kao, M.S., 2000. In-plane vibration of laminated curved beams with variable curvature by dynamic stiffness analysis. *Composite Structures* 50 (2), 103–114.
- Washizu, K., 1982. *Variational Methods in Elasticity and Plasticity*, third ed. Pergamon Press, Oxford.
- Wasserman, Y., 1977. The influence of the behaviour of the load on the frequencies and critical loads of arches with flexibility supported ends. *Journal of Sound and Vibration* 54, 515–526.
- Wempner, G.A., Kesti, N.E., 1962. On the buckling of circular arches and rings. 4th US National Congress of Applied Mechanics. pp. 843–849.
- Yang, M.C., 2002. Dynamic and buckling behaviors of preloaded arches with shear deformation. M.S. Thesis, National Chiao Tung University, Taiwan (in Chinese).